Hobit confers tissue-dependent programs to type 1 innate lymphoid cells

Kentaro Yomogida[a,b], Tarin M. Bigley[b], Tihana Trsan[a], Susan Gilfillan[a], Marina Cella[a], Wayne M. Yokoyama[c], Takeshi Egawa[a], and Marco Colonna[a,1]

[a]Department of Pathology and Immunology, Washington University School of Medicine, St. Louis, MO 63110; [b]Department of Pediatrics, Washington University School of Medicine, St. Louis, MO 63110; and [c]Rheumatology Division, Washington University School of Medicine, St. Louis, MO 63110

Contributed by Marco Colonna; received September 30, 2021; accepted November 3, 2021 by Editorial Board Members Bojan Polic and Chiara Romagnani

Identification of type 1 innate lymphoid cells (ILC1s) has been problematic. The transcription factor Hobit encoded by *Zfp683* has been proposed as a major driver of ILC1 programs. Using *Zfp683* reporter mice, we showed that correlation of Hobit expression with ILC1s is tissue- and context-dependent. In liver and intestinal mucosa, *Zfp683* expression correlated well with ILC1s; in salivary glands, *Zfp683* was coexpressed with the natural killer (NK) master transcription factors Eomes and TCF1 in a unique cell population, which we call ILC1-like NK cells; during viral infection, *Zfp683* was induced in conventional NK cells of spleen and liver. The impact of *Zfp683* deletion on ILC1s and NK cells was also multifaceted, including a marked decrease in granzyme- and interferon-gamma (IFNγ)–producing ILC1s in the liver, slightly fewer ILC1s and more Eomes$^+$ TCF1$^+$ ILC1-like NK cells in salivary glands, and only reduced production of granzyme B by ILC1 in the intestinal mucosa. NK cell–mediated control of viral infection was unaffected. We conclude that Hobit has two major impacts on ILC1s: It sustains liver ILC1 numbers, while promoting ILC1 functional maturation in other tissues by controlling TCF1, Eomes, and granzyme expression.

innate lymphoid cells | natural killer cells | Hobit | Eomes | liver

Innate lymphoid cells (ILCs) comprise a diverse group of lymphocytes devoid of rearranged antigen receptors. ILCs are classified into three groups based on their functional programs. The type 1 ILC (ILC1) program driven by Tbet culminates with production of interferon-gamma (IFNγ); the ILC2 program dictated by GATA3 promotes secretion of interleukin-5 (IL-5) and IL-13; the ILC3 program driven by Rorγt leads to production of IL-17 and IL-22 (1–3). In mice, ILC1s and natural killer (NK) cells both require Tbet, produce IFNγ, and express the cell-surface markers NKp46 and NK1.1. Given these similarities, distinguishing ILC1s from NK cells has been problematic (4–6). One important distinction between ILC1s and NK cells is that ILC1s are mainly tissue-resident, whereas NK cells circulate in the blood (7). Therefore, ILC1s provide a local source of IFNγ for prompt control of intracellular pathogens, whereas NK cells recruited from the blood provide a second wave of IFNγ (8). Moreover, NK cells are thought to be more cytotoxic than ILC1s due to superior production of perforin and granzymes, though recent studies have challenged this view (9, 10). Phenotypically, various specific cell-surface markers have been identified for each cell type. CD49a, CD200R1, CD69, CD103, and CD127 are mainly expressed in ILC1s (11), while NK cells express CD49b, CD62L, as well as NK cell receptors of the immunoglobulin and C-type lectin families with a semiclonal distribution (12, 13). However, the expression of these markers can vary among tissues and can be acquired or modulated in pathological conditions, such as viral infections and tumors.

ILC1s and NK cells follow different developmental trajectories. NK cells originate from an early common innate lymphoid progenitor, whereas all ILCs derive from a downstream Id2$^+$ common helper innate lymphoid progenitor (5, 14, 15); however, recent reports have identified a shared progenitor that gives rise to both ILC1s and NK cells (16). Regardless of their progenitor, NK cells and ILC1s express unique transcription factors that shape their identities. NK cells depend on Eomes for development, whereas ILC1s are Eomes-independent (17). The transcriptional regulator Hobit, encoded by the gene *Zfp683*, is highly expressed in ILC1s and is required for liver ILC1s but not NK cells (18). In a recent single-cell RNA-sequencing (scRNA-seq) analysis of the ILC1–NK spectrum in multiple tissues, we confirmed that ILC1s and NK cells are generally associated with expression of Hobit and Eomes, respectively, but also noticed a considerable tissue heterogeneity of ILC1s and NK cells (19). For example, salivary glands and uterus contain a unique cell population that expresses both Eomes and Hobit, as well as the transcription factor TCF1. We refer to these cells as "ILC1-like NK cells." These cells are also unique for their independence from NFIL3 (20–22), a transcriptional repressor required by both NK cells and ILC1s for development (23–27). Thus, Hobit may not be a univocal driver of ILC1s.

To evaluate the association of Hobit with ILC1s and its impact on their development and functions, we generated a Hobit reporter mouse that identifies cells expressing Hobit within the ILC1–NK spectrum, as well as a Hobit fate-map mouse that identifies ILCs and NK cells that have expressed Hobit at any time of their development. Using these tools, we showed that Hobit association with ILC1s and their cell-surface

Significance

Innate responses against viral infection and other intracellular pathogens rely on immune cells that are capable of lysing infected cells and producing interferon-gamma (IFNγ). These cells encompass two major cell lineages: natural killer (NK) cells and type 1 innate lymphoid cells (ILC1s). While NK cells have been extensively characterized, identification of ILC1s and their distinction from NK cells are less clear. The transcription factor Hobit encoded by *Zfp683* has been put forth as a prototypic feature of ILC1s. By analyzing *Zfp683* reporter, fate-map, and -deficient mice, we demonstrate that the impact of Hobit on ILC1 identity and transcriptional and functional programs is tissue- and context-dependent. Thus, ILC1s adapt to local stimuli and tailor their responses to the tissue niche.

Author contributions: K.Y. and M. Colonna designed research; K.Y., T.M.B., and T.T. performed research; S.G., W.M.Y., and T.E. contributed new reagents/analytic tools; K.Y., T.M.B., and M. Cella analyzed data; and K.Y., M. Cella, and M. Colonna wrote the paper.

Reviewers: B.P., Sveuciliste u Rijeci Zavod za Histologiju i Embriologiju; and C.R., Deutsches Rheuma-Forschungszentrum.

The authors declare no competing interest.

[1]To whom correspondence may be addressed. Email: mcolonna@wustl.edu.

This article contains supporting information online at http://www.pnas.org/lookup/suppl/doi:10.1073/pnas.2117965118/-/DCSupplemental.

Published December 8, 2021.

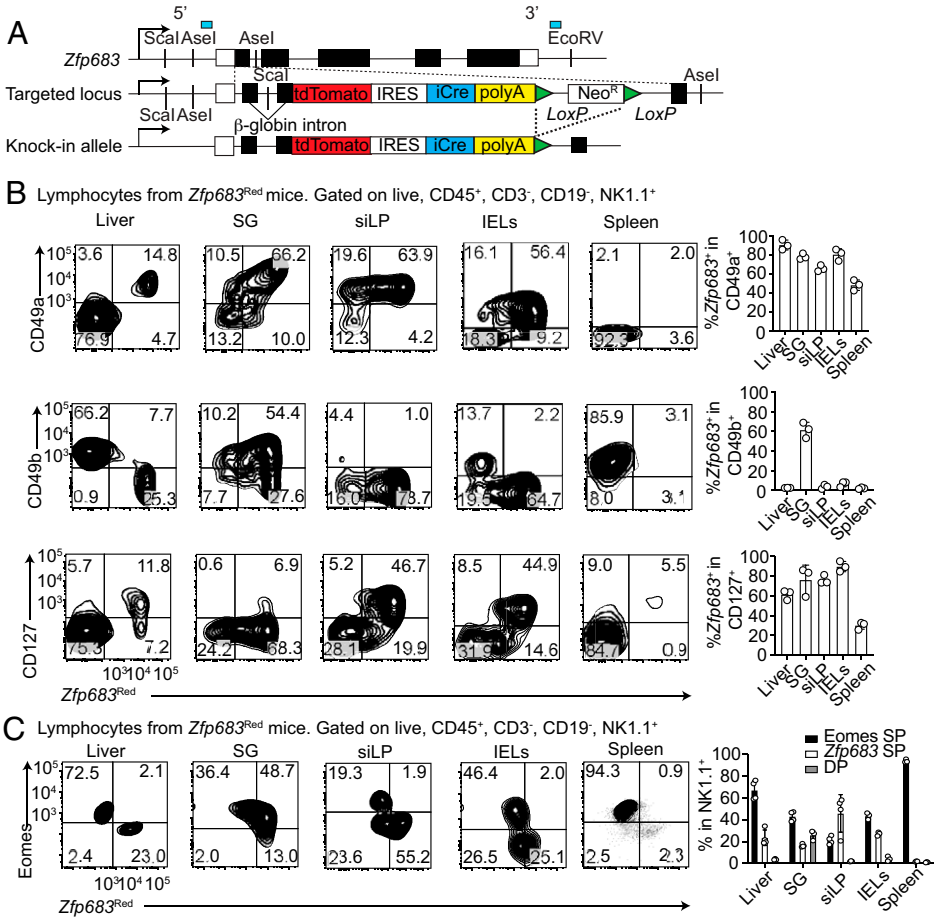

Fig. 1. *Zfp683* and Eomes define ILC1s and NK cells across tissues. (*A*) Schematic of targeting construct. (*B*) Representative flow cytometric dot plots and quantification of *Zfp683*$^+$ cells among live, CD45$^+$Lin$^-$NK1.1$^+$CD49a$^+$, CD49b$^+$, or CD127$^+$ cells in the indicated organs. Single-cell suspensions were obtained from heterozygous *Zfp683*^{Red} mice. IELs, intraepithelial lymphocytes; SG, salivary gland; siLP, small intestinal lamina propria. Data are representative of two independent experiments (n = 3 or 4). Data represent mean ± SEM. (*C*) Expression of Eomes and *Zfp683* in single-cell suspensions from different organs of *Zfp683*^{Red} heterozygous mice, and their quantification among NK1.1$^+$ cells gated as in *B*. DP, double-positive; SP, single positive. Data represent mean ± SEM. Data are representative of two independent experiments (n = 3 or 4).

markers varies in different tissues. We also showed that Hobit fate-mapped$^+$ cells can be found in ILC1s and a subset of ILC3s but not in NK cells, demonstrating that ILC1s represent a lineage distinct from NK cells, which can in part convert into ILC3s. scRNA-seq and flow cytometric analyses of mice with a conditional deletion of *Zfp683* in the ILC1–NK spectrum showed that the impact of Hobit on ILC1s also varies in different tissues. Lack of Hobit has the following effects: 1) markedly reduced numbers of two ILC1 subsets specialized in either granzyme or IFNγ production in the liver; 2) slightly fewer ILC1s that fail to effectively produce granzyme B along with more Eomes- and TCF1-driven ILC1-like NK cells in the salivary gland; and 3) only defective expression of granzyme B by ILC1s in the small intestine. Finally, we found that murine cytomegalovirus (MCMV) infection induced Hobit expression in spleen and liver NK cells, although it was not necessary to sustain NK cell–mediated control of viral infection in liver. We conclude that the expression and impact of Hobit are tissue- and context-dependent in ILC1s and NK cells.

Results

Hobit Association with ILC1 Surface Markers Varies in Different Organs. To trace cells expressing Hobit and define their features compared with other innate lymphocytes, we generated knockin/knockout Hobit reporter mice. We inserted a tandem dimer red fluorescent protein (tdTomato) and a Cre recombinase linked by an internal ribosomal entry site (IRES) at the translation initiation site of the *Zfp683* gene encoding Hobit (Fig. 1*A*). We called these mice *Zfp683*^{Red}. The size of the *Zfp683*$^+$ population among Lin$^-$NK1.1$^+$ cells differed in various tissues; *Zfp683*$^+$ cells comprised a large fraction of NK1.1$^+$ cells in liver, salivary glands, intestinal lamina propria, and intestinal epithelium, but were scarce in the spleen (Fig. 1*B*). We next investigated the association of Hobit with ILC1 markers in these tissues. CD49a and CD49b are often used to identify ILC1s and NK cells, respectively (1). In liver, *Zfp683*$^+$ cells coincided with CD49a$^+$ cells, whereas CD49b$^+$ cells encompassed *Zfp683*$^-$ cells. In the lamina propria and the epithelial layer of intestinal mucosa, NK1.1$^+$ cells were mainly CD49a$^+$ and ∼60 to 80% of these cells expressed *Zfp683* (Fig. 1*B*). In salivary glands, the majority of NK1.1$^+$ cells expressed both CD49a and CD49b as well as *Zfp683*, with only relatively small fractions of CD49a$^+$ or CD49b$^+$ cells lacking *Zfp683* (Fig. 1*B*). The spleen contained mainly CD49b$^+$ cells, which were largely *Zfp683*$^-$ (Fig. 1*B*). The receptor for IL-7 (CD127) is another marker reported to be expressed by most ILCs (11). A large proportion of *Zfp683*$^+$ cells expressed CD127 in the intestinal lamina propria and epithelium; around 50 to 70% of *Zfp683*$^+$ cells expressed CD127 in the liver. Only a very small fraction of salivary glands and splenic NK1.1$^+$ cells (2 to 7%) expressed CD127, most of which expressed *Zfp683*. These results indicate

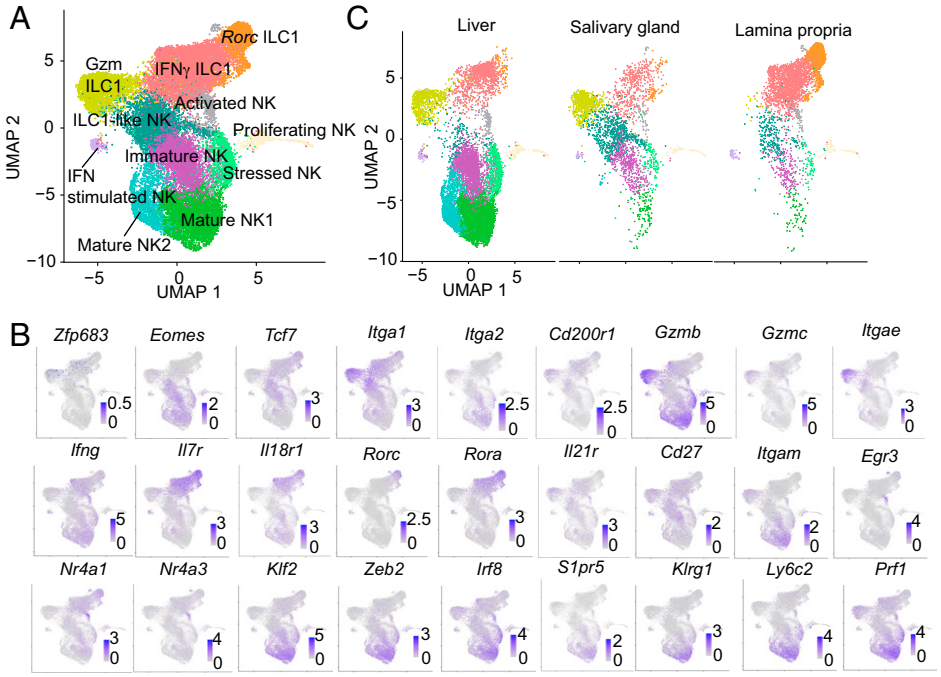

Fig. 2. scRNA-seq delineates previously unappreciated ILC1 and NK cell subpopulations. (*A*) UMAP plot of 17,660 CD3$^-$NK1.1$^+$ cells from multiple tissues. Each cluster was annotated based on differentially expressed genes. (*B*) UMAP plots of representative selected genes that discriminate among the identified clusters. (*C*) UMAP plots of CD3$^-$NK1.1$^+$ cells from the indicated tissues.

that the commonly used cell markers CD49a and CD127 identify *Zfp683*$^+$ ILC1s only in part, as the association of these markers with *Zfp683* expression varies in different tissues.

Hobit and Eomes Are Mutually Exclusively Expressed in Most Tissues. If Hobit and Eomes identify ILC1s and NK cells, respectively, their expression should be mutually exclusive. We examined Lin$^-$NK1.1$^+$ cells for intracellular content of Eomes versus *Zfp683* expression in various tissues of *Zfp683*^{Red} mice. Cells in liver, intestinal lamina propria, intestinal epithelium, and spleen exclusively expressed either Eomes or *Zfp683* (Fig. 1*C*). This pattern corroborated the existence of *Zfp683*$^+$ ILC1s distinct from Eomes$^+$ NK cells. However, about 30 to 50% of NK1.1$^+$ cells in salivary glands expressed both Eomes and *Zfp683* (Fig. 1*C*), as well as CD49a (*SI Appendix*, Fig. S1), and therefore could not be rigorously classified as NK cells or ILC1s; we refer to these cells as ILC1-like NK cells.

scRNA-Seq Reveals ILC1 Subsets Differentially Represented in Distinct Tissues. To further investigate the expression of Hobit across tissue ILC1s and its association with different markers, we isolated Lin$^-$NK1.1$^+$ cells from liver, salivary glands, and intestinal lamina propria, which contain the largest fraction of *Zfp683*$^+$ cells, and performed scRNA-seq using the 10X Chromium platform. We profiled a total of quality-controlled 17,660 cells (*SI Appendix*, Table S1) that were visualized using the uniform manifold approximation and projection (UMAP) method, regardless of the tissue origin. ILC1 and NK cell clusters were defined based on the top 20 differentially expressed genes (Fig. 2 *A* and *B* and *SI Appendix*, Fig. S2). We promptly identified ILC1 and NK cell clusters based on expression of *Zfp683* and *Eomes*, respectively, as well as ILC1-like NK cells expressing both *Zfp683* and *Eomes*. ILC1-like NK cells also expressed *Tcf7*, which encodes TCF1. This distinction was consistent with the distribution of *Itga1* (for CD49a) and *Itga2* (for CD49b). *Cd200r1*, a marker of ILC1s (8), overlapped with *Zfp683* and *Itga1*. We further distinguished three groups of ILC1s: granzyme-producing ILC1s (Gzm ILC1), IFNγ-producing ILC1s (IFNγ ILC1), and *Rorc* ILC1s (*Rorc* ILC1). Gzm$^+$ ILC1s expressed messenger RNA (mRNA) for granzymes (*Gzma*, *Gzmb*, *Gzmc*), as well as *Itgae* (for CD103), *Tyrobp* (for DAP12), and the inhibitory receptor *Lag3* (Fig. 2 *A* and *B* and *SI Appendix*, Fig. S2). *Gzmc* was uniquely expressed by ILC1s, whereas *Gzmb* was expressed in both ILC1s and NK cells. Gzm ILC1s expressed less perforin mRNA (*Prf1*) than NK cells, suggesting a lower cytotoxic capacity. However, Gzm ILC1s abundantly expressed the IL-21 receptor transcript (*Il21r*), which has been shown to enhance cytotoxicity (28). Thus, ILC1 lytic ability may depend on the levels of IL-21 in the tissue. IFNγ ILC1s were discriminated by high expression of *Ifng*, *Xcl1*, *Ltb*, as well as *Il7r*, *Il18r1*, and *Cd226* (Fig. 2 *A* and *B* and *SI Appendix*, Fig. S2). The *Rorc* ILC1 cluster expressed some ILC3 signature genes, including *Rorc*, *Rora*, *Maf*, *Tmem176a*, *Tmem176b*, *Lta*, and *Ltb*. Despite this signature, *Rorc* ILC1s expressed no *Il17* or *Il22*, while *Ifng* levels were similar to the other ILC1 clusters (Fig. 2 *A* and *B* and *SI Appendix*, Fig. S2). Thus, *Rorc* ILC1s may encompass ILC1s that originate from conversion of Rorγt$^+$ ILC3s, commonly known as "exILC3s" (29), or from a Rorγt$^+$ progenitor.

NK cells included three major clusters: immature NK (iNK) cells expressing *Cd27*, mature NK (mNK) cells expressing *Itgam* (for CD11b), and activated NK cells expressing various cytokines and chemokine genes and the transcription factors *Egr3*, *Nr4a1*, and *Nr4a3* (Fig. 2*B* and *SI Appendix*, Fig. S2). iNK cells expressed *Tcf7*, indicating a program for proliferation and lymph node homing (30). Among mNK cell signature genes, *Klf2*, *Zeb2*, *Irf8*, *S1pr5*, *Klrg1*, *Ly6c2*, and *Prf1* indicated programs for effector function and recirculation (31–34). The distinction between mNK1 and mNK2 clusters was based on slightly different expression levels of mNK signature genes. We also identified a "stressed" NK cell cluster based on high expression of the stress response genes *Hspe1* and *Hsp90ab1*, as well as a cluster of proliferating NK cells expressing *Mki67*, *Tuba1b*, *Stmn1*, and

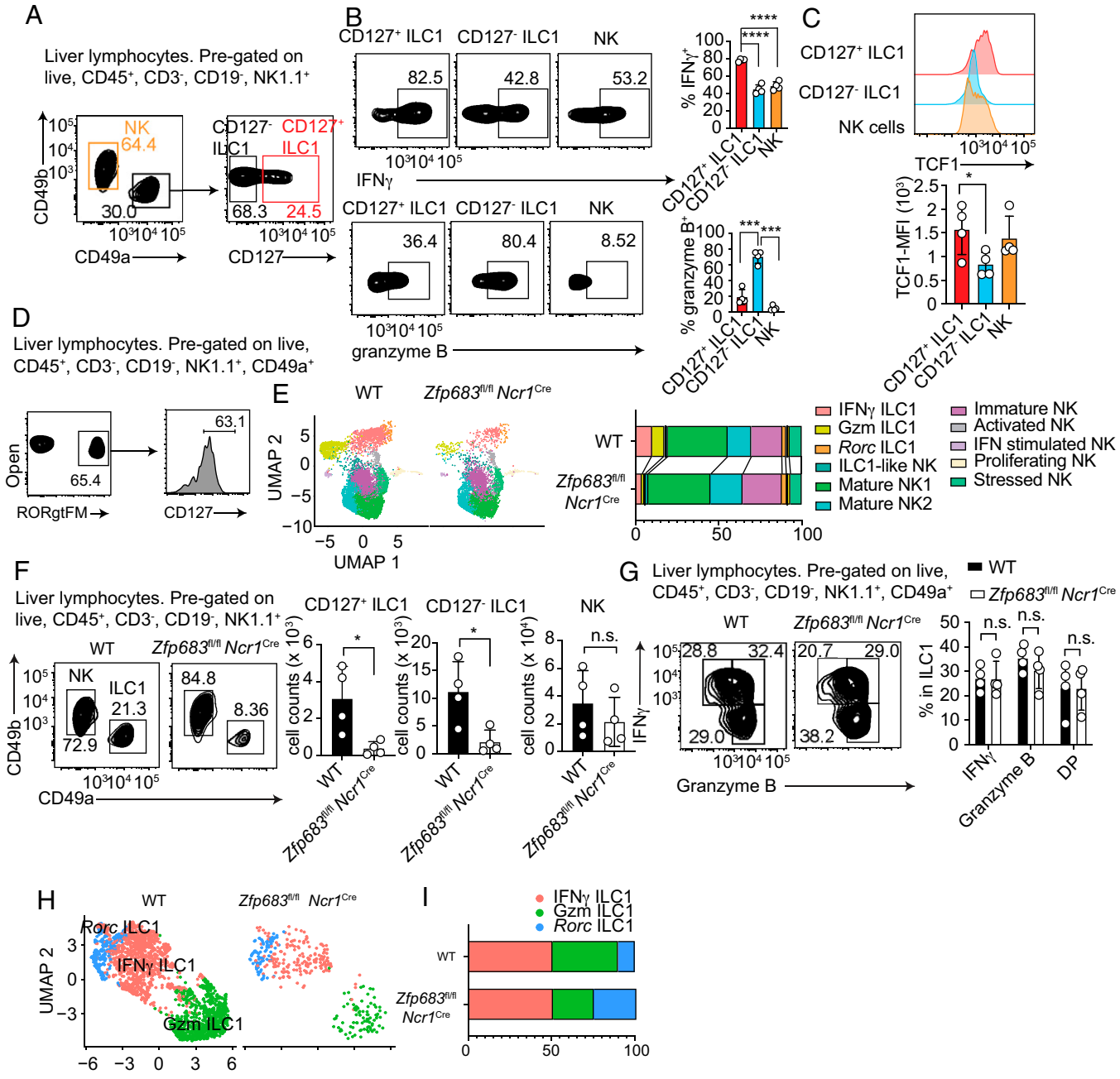

Fig. 3. CD127 expression identifies at least two liver ILC1 subsets. (*A*) Representative flow cytometric gating strategy for liver NK cell and ILC1 subsets and expression of CD127 on CD49a$^+$CD49b$^-$ ILC1s. (*B*) Representative flow cytometric dot plots and quantification of IFNγ and granzyme B expression in the indicated populations. It should be noted that liver NK cells include both iNK and mNK cells, which produce distinct amounts of IFNγ; therefore, the values of IFNγ depicted represent an average of the entire NK population. (*C*) Representative flow cytometric histogram plots and quantification of TCF1 protein expression in the indicated populations. (*D*) Representative flow cytometric dot plots showing expression of CD127 on RORγt fate-map (RORγtFM) liver CD49a$^+$ ILC1s. (*E*) UMAP plots and cluster representation among CD3$^-$NK1.1$^+$ cells from wild-type or *Zfp683*$^{fl/fl}$ *Ncr1*^{Cre} mice. (*F*) Representative flow cytometric dot plots and total cell counts of the indicated populations from wild-type or *Zfp683*$^{fl/fl}$ *Ncr1*^{Cre}mice. (*G*) Representative flow cytometric dot plots and quantification showing the expression of IFNγ and granzyme B in the indicated populations from wild-type or *Zfp683*$^{fl/fl}$ *Ncr1*^{Cre} mice. (*H* and *I*) UMAP plots (*H*) and cluster proportion (*I*) of liver ILC1s from wild-type or *Zfp683*$^{fl/fl}$ *Ncr1*^{Cre} mice. Data from *A*–*D*, *F*, and *G* are representative of two independent experiments ($n = 4$). Data represent mean ± SEM. *$P < 0.05$, ***$P < 0.001$, ****$P < 0.0001$; n.s., not significant. MFI, mean fluorescence intensity; WT, wild type.

Tubb5 (*SI Appendix*, Fig. S2). We also detected a small NK cell cluster enriched for the IFN-stimulated genes (*Ifit1*, *Ifit3*, *Ifi209*, *Irf7*, *Iigp1*, *Ifi208*, *Isg20*), which was termed "IFN-stimulated" NK cells (*SI Appendix*, Fig. S2). The representation of the ILC1 clusters was skewed in a tissue-specific manner. The liver included all major ILC1 subsets, Gzm ILC1s, IFNγ ILC1s, and *Rorc* ILC1s; salivary glands contained a relatively large population of ILC1-like NK cells; and IFNγ ILC1s and *Rorc* ILC1s predominated in the intestinal lamina propria (Fig. 2*C*). Together, these data show that although all ILC1s express Hobit, they include disparate subsets with specialized effector functions, which are differentially represented in various tissues.

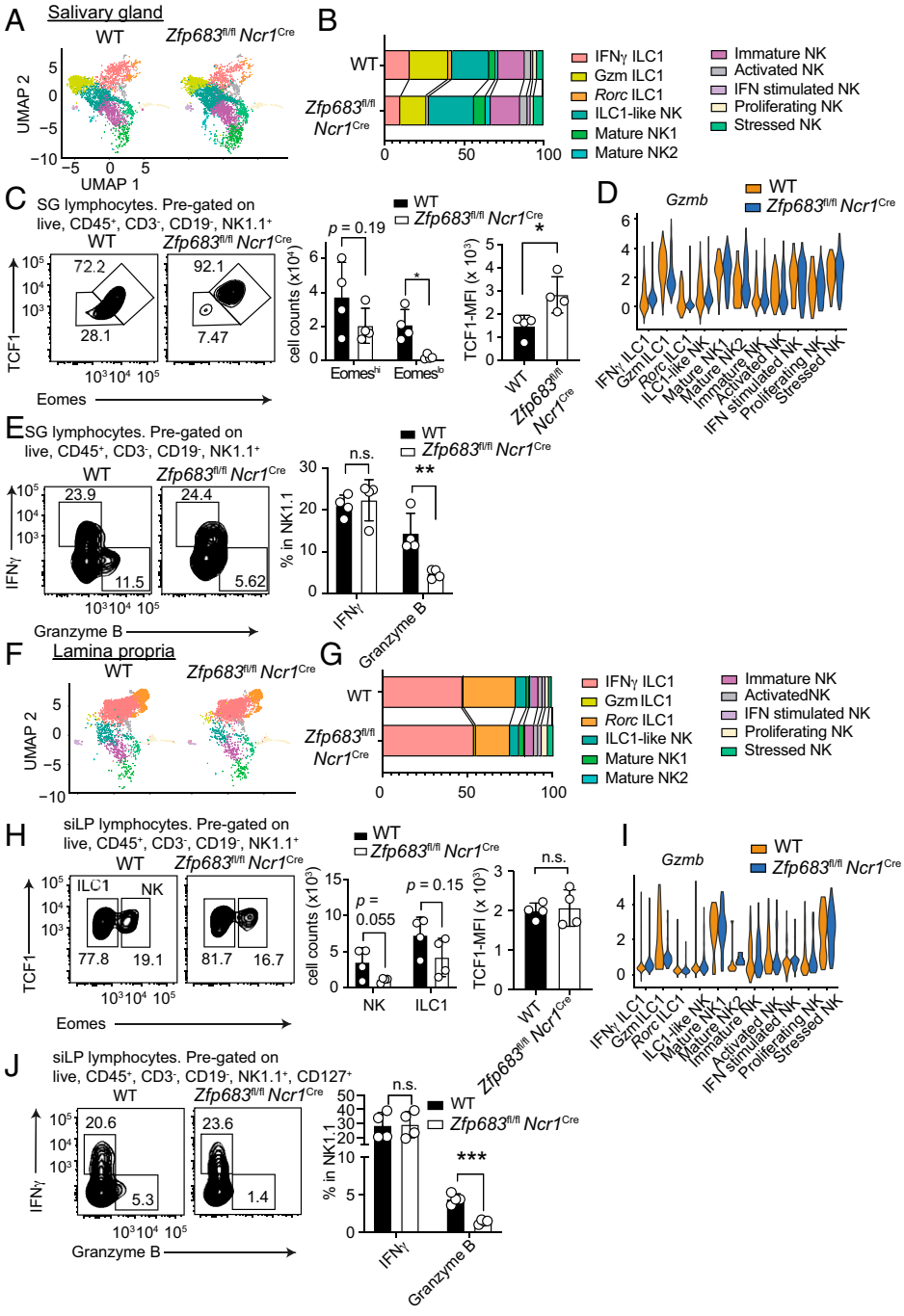

Fig. 4. Hobit differentially regulates expression of granzyme B, TCF1, and Eomes in salivary gland and lamina propria ILC1s. (*A* and *B*) UMAP plots (*A*) and cluster representation (*B*) of salivary gland CD3$^-$NK1.1$^+$ cells from wild-type or *Zfp683$^{fl/fl}$ Ncr1^{Cre}* mice. (*C*) Representative flow cytometric dot plots and quantification of Eomes$^{hi/lo}$ and TCF1 expression cells among NK1.1$^+$ cells in salivary glands from wild-type or *Zfp683$^{fl/fl}$ Ncr1^{Cre}* mice. (*D*) Violin plots of granzyme B expression levels in each cluster of salivary gland CD3$^-$NK1.1$^+$ cells. (*E*) Representative flow cytometric dot plots and quantification of IFNγ and granzyme B in the indicated NK1.1$^+$ populations of salivary glands from wild-type or *Zfp683$^{fl/fl}$ Ncr1^{Cre}* mice. (*F* and *G*) UMAP plots (*F*) and cluster representation (*G*) in lamina propria CD3$^-$NK1.1$^+$ cells from wild-type or *Zfp683$^{fl/fl}$ Ncr1^{Cre}* mice. (*H*) Representative flow cytometric dot plots showing expression of Eomes and TCF1 and quantification of absolute numbers of ILC1s and NK cells and of TCF1 expression in the indicated populations of lamina propria NK1.1$^+$ cells from wild-type or *Zfp683$^{fl/fl}$ Ncr1^{Cre}* mice. (*I*) Violin plots of granzyme B expression levels in each cluster of intestinal lamina propria CD3$^-$NK1.1$^+$ cells. (*J*) Representative flow cytometric dot plots and quantification of IFNγ and granzyme B in the indicated lamina propria NK1.1$^+$ populations from wild-type or *Zfp683$^{fl/fl}$ Ncr1^{Cre}* mice. Data represent mean ± SEM. *$P < 0.05$, **$P < 0.01$, ***$P < 0.001$; n.s., not significant. (*C*, *E*, *H*, and *J*) Data are representative of two independent experiments ($n = 4$). (*E* and *J*) NK cells and ILC1s were stimulated with IL-12 and IL-18. All flow cytometric plots were pregated with the indicated markers. Data represent mean ± SEM.

Liver Gzm and IFNγ ILC1s Require Hobit. We sought to validate liver Gzm and IFNγ ILC1s by flow cytometry. We examined liver Lin$^-$NK1.1$^+$ for surface expression of CD49a, CD49b, and CD127 and intracellular content of IFNγ and granzyme B. CD49a$^+$CD127$^+$ ILC1s produced more IFNγ but less granzyme B than did CD49a$^+$CD127$^-$ ILC1s (Fig. 3 *A* and *B*). Since TCF1 limits granzyme B expression in NK cells (35), we also analyzed intracellular levels of TCF1 in ILC1s.

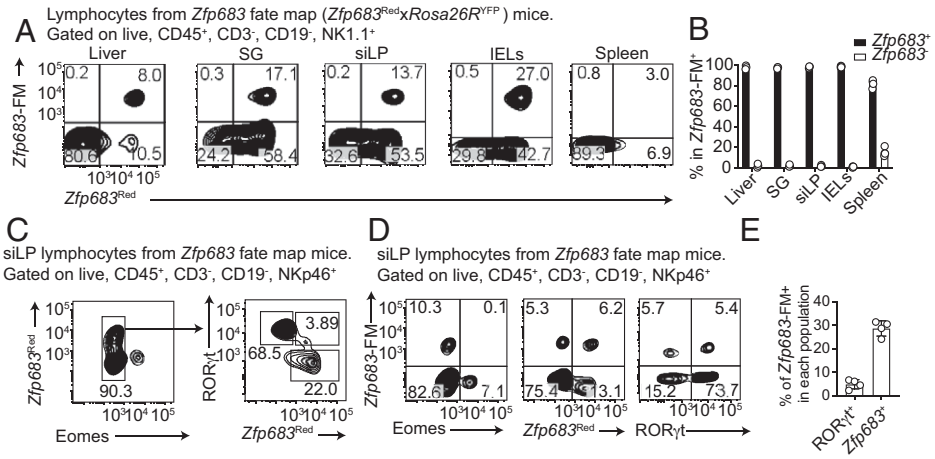

Fig. 5. NK cells and ILC1s are independent lineages, but a small portion of ILC1s convert to ILC3s. (*A* and *B*) Representative flow cytometric dot plots (*A*) and quantification (*B*) of Hobit-expressing (*Zfp683*^{Red}) versus Hobit fate-map (*Zfp683*^{FM}) among NK1.1$^+$ cells in different organs. Single-cell suspensions were obtained from heterozygous *Zfp683*^{Red} mice. (*C*) Representative flow cytometric dot plots showing expression of Hobit (*Zfp683*^{Red}), Eomes, and RORγt among NKp46$^+$ cells of the small intestinal lamina propria, which include ILC1s, ILC3s, and NK cells. (*D* and *E*) Representative flow cytometric dot plots (*D*) and quantification (*E*) showing expression of Hobit fate-map (*Zfp683*^{FM}) cells coexpressing RORγt or *Zfp683*. Data are representative of at least two independent experiments (n = 3 or 4). Data represent mean ± SEM.

In line with elevated granzyme B production, CD49a$^+$CD127$^-$ ILC1s expressed less TCF1 than did CD49a$^+$CD127$^+$ ILC1s (Fig. 3*C*). We conclude that liver ILC1s include a CD127$^+$TCF1^{hi} subset specialized in IFNγ production and a CD127$^-$TCF1^{lo} subset specialized in granzyme production. To validate liver *Rorc* ILC1s, we examined liver ILC1s in *Rorc-Cre* mice crossed with *Rosa26R*^{YFP} mice (*Rorc*FM), in which cells that express or have expressed Rorγt$^+$ can be fate-mapped as YFP$^+$. A considerable percentage of liver CD49a$^+$ ILC1s were *Rorc*FM$^+$ (Fig. 3*D*), suggesting that they derive, at least in part, from the conversion of Rorγt$^+$ ILC3s or from a Rorγt$^+$ progenitor.

Since it has been shown that Hobit is required for liver ILC1s (18), we asked whether IFNγ ILC1, Gzm ILC1, and *Rorc* ILC1 subsets depend on it. We generated *Zfp683*$^{fl/fl}$ mice and crossed them with *Ncr1*^{Cre} mice, which express Cre recombinase in NK cells and ILC1s, thereby abrogating Hobit expression in both populations. scRNA-seq analysis of NK1.1$^+$ cells from *Zfp683*$^{fl/fl}$ *Ncr1*^{Cre} versus *Zfp683*$^{fl/fl}$ mice revealed a reduction of both Gzm and IFNγ ILC1s, whereas *Rorc* ILC1s seemed unaffected (Fig. 3*E*). Flow cytometric analysis corroborated a marked reduction of both CD127$^+$ and CD127$^-$ ILC1s in *Zfp683*$^{fl/fl}$ *Ncr1*^{Cre} mice, while NK cells were not significantly affected (Fig. 3*F*). The few remaining ILC1s present in *Zfp683*$^{fl/fl}$ *Ncr1*^{Cre} mice maintained production of IFNγ and granzyme B, perhaps representing cells escaped from Cre recombination (Fig. 3*G*).

To further examine the impact of *Zfp683* deletion in liver ILC1s, we reclustered ILC1s from our scRNA-seq data (Fig. 3 *H* and *I* and *SI Appendix*, Fig. S3). This analysis corroborated the presence of Gzm, IFNγ, and *Rorc* ILC1s and the strong reduction of Gzm ILC1 and IFNγ ILC1 clusters in the absence of *Zfp683*. However, we noticed a small relative increase of *Rorc* ILC1s in *Zfp683*$^{fl/fl}$ *Ncr1*^{Cre} samples, suggesting that this subset may be less affected or unaffected by *Zfp683* deletion. All ILC1 clusters expressed *Zfp683* and *Ifng*. *Rorc* ILC1s shared expression of *Kit*, *Il7r*, and *Tcf7* with IFNγ ILC1s, whereas Gzmb was preferentially expressed in Gzm ILC1s. Together, these data demonstrate that liver ILC1s include two functionally polarized ILC1 subsets that are Hobit-dependent and a third Hobit-independent subset that may derive from Rorγt$^+$ ILC3s or from a Rorγt$^+$ progenitor.

ILC1 Requirement for Hobit Varies in Different Tissues. We further examined the impact of Hobit deficiency on ILC1s in salivary glands and intestinal lamina propria by scRNA-seq of Lin$^-$NK1.1$^+$ cells isolated from *Zfp683*$^{fl/fl}$ *Ncr1*^{Cre} mice and control *Zfp683*$^{fl/fl}$ mice. Salivary glands harbored both Gzm and IFNγ ILC1s, as well as ILC1-like NK cells. Fewer Gzm and IFNγ ILC1s and more ILC1-like NK cells were present in *Zfp683*$^{fl/fl}$ *Ncr1*^{Cre} mice than in *Zfp683*$^{fl/fl}$ mice, whereas NK cells were similarly represented in the two (Fig. 4 *A* and *B*). We confirmed this observation in *Zfp683*^{Red} mice. Since the reporter cassette disrupts the *Zfp683* allele, homozygous *Zfp683*^{Red} mice lack functional Hobit-encoding genes; again, fewer ILC1s and more ILC1-like NK cells were found in the salivary glands of homozygous than in heterozygous *Zfp683*^{Red} mice (*SI Appendix*, Fig. S4).

Since ILC1s are TCF1^{lo} Eomes$^-$, whereas ILC1-like NK cells are TCF1^{hi} Eomes$^+$ (Fig. 2), we further investigated the impact of Hobit deficiency on TCF1 and Eomes by flow cytometry. A reduction of Eomes$^-$ TCF1^{lo} cells paralleled by an increase in Eomes$^+$ TCF1^{hi} ILC1-like NK cells was noted in the salivary glands of *Zfp683*$^{fl/fl}$ *Ncr1*^{Cre} mice (Fig. 4*C*). These results suggest that Hobit negatively regulates expression of Eomes and TCF1 in salivary gland ILC1s and ILC1-like NK cells. We also examined the impact of *Zfp683* deletion on effector functions: violin plots indicating the expression of *Gzmb* in each ILC1–NK subset showed a clear reduction of *Gzmb* in ILC1s from *Zfp683*$^{fl/fl}$ *Ncr1*^{Cre} mice (Fig. 4*D*). Flow cytometric analysis validated that *Zfp683* deletion led to reduced intracellular content of granzyme B, whereas IFNγ was unchanged (Fig. 4*E*).

scRNA-seq exposed no marked impact of *Zfp683* deletion on the abundance of ILC1s in the Lin$^-$NK1.1$^+$ cells of the intestinal lamina propria (Fig. 4 *F* and *G*). Moreover, flow cytometric analysis corroborated that *Zfp683* deletion had no obvious impact on Eomes or TCF1 expression (Fig. 4*H*). However, granzyme B mRNA and protein expression were significantly impaired in *Zfp683*-deficient lamina propria ILC1s, as observed in salivary glands (Fig. 4 *I* and *J*). Overall, these results demonstrate that the impact of *Zfp683* deletion on the representation of ILC1 subsets and their expression of TCF1, Eomes, and granzyme B varies considerably depending on the tissue.

ILC1s Show Limited Conversion into ILC3s in Steady State. Several studies of ILC1–NK cell lineage relationships have proposed that ILC1s and NK cells are distinct lineages (14, 15, 17),

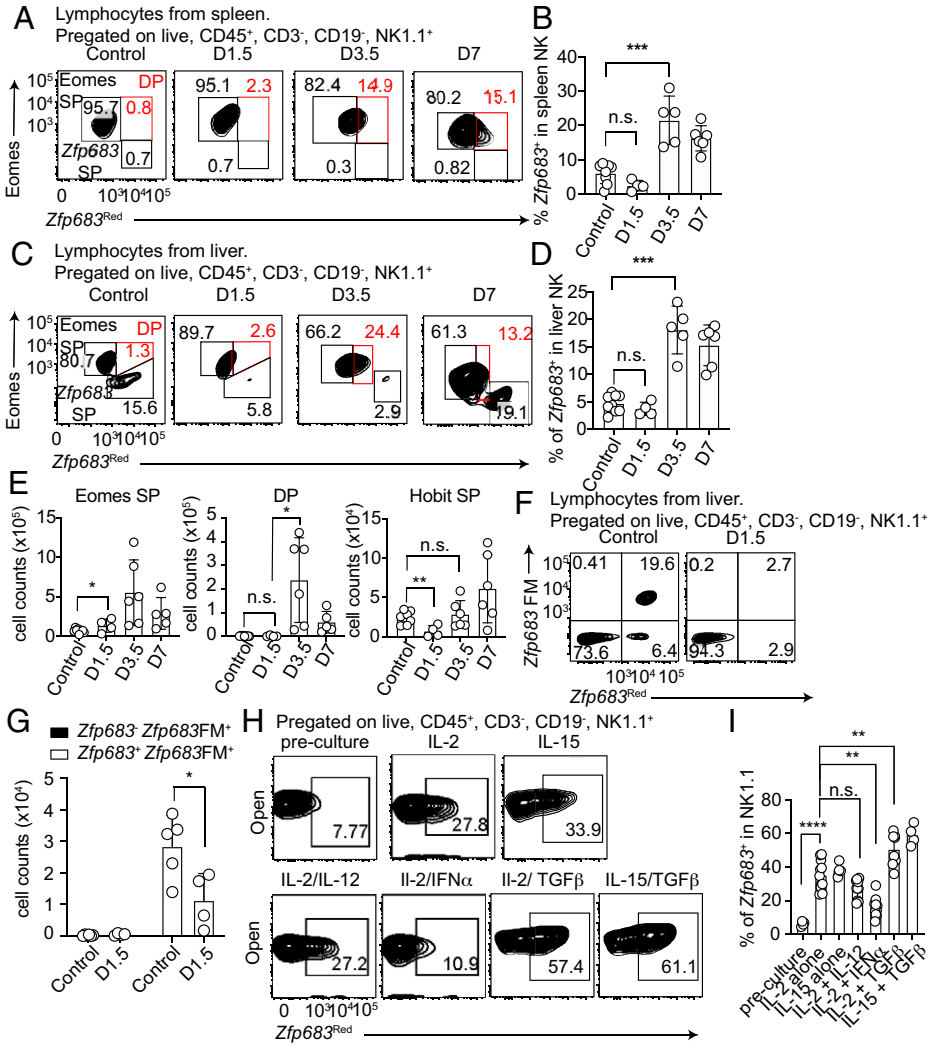

Fig. 6. MCMV infection induces Hobit expression in NK cells. (*A* and *B*) Representative flow cytometric dot plots (*A*) and quantification (*B*) of Hobit-expressing (*Zfp683*^{Red}) splenic NK cells at different time points after MCMV i.p. infection. (*C* and *D*) Representative dot plots of Hobit-expressing (*Zfp683*^{Red}) and Eomes-expressing liver ILC1s and NK cells (*C*) and their quantification (*D*) at the indicated time points after MCMV i.p. infection in heterozygous *Zfp683*^{Red} mice. (*E*) Absolute cell numbers of the indicated populations in the liver at the indicated time points post–MCMV i.p. infection. (*F* and *G*) Representative flow cytometric dot plots (*F*) and absolute cell counts (*G*) of Hobit-expressing (*Zfp683*^{Red}) or Hobit fate map (*Zfp683*^{FM}) among liver NK1.1$^+$ cells at 1.5 d post–MCMV infection. (*H* and *I*) Representative flow cytometric dot plots (*H*) and quantification (*I*) of Hobit-expressing (*Zfp683*^{Red}) in splenic NK1.1$^+$ cells after 72 h in culture with the indicated cytokines. Data are representative of at least two independent experiments (n = 5 to 8). Data represent mean ± SEM. *P < 0.05, **P < 0.01, ***P < 0.001, ****P < 0.0001; n.s., not significant.

although other reports disagree (16). Prior studies utilized either adoptive cell transfer or ex vivo culture systems but did not analyze lineage relationships in unperturbed physiological conditions. To overcome these limitations, we crossed *Zfp683*^{Red} mice with *Rosa26R*^{YFP} mice to generate *Zfp683* fate-map (*Zfp683*^{FM}) mice, in which cells that currently express *Zfp683* are Tomato$^+$, while cells that have expressed *Zfp683* at any time point of their development are YFP$^+$. We focused on Lin$^-$NK1.1$^+$ cells, which include ILC1s and NK cells. Analysis of *Zfp683*$^{FM+}$ (YFP$^+$) versus *Zfp683*$^+$ (tdTomato$^+$) Lin$^-$NK1.1$^+$ cells in various tissues revealed that *Zfp683*$^{FM+}$ cells are almost exclusively detected within the *Zfp683*$^+$ population, while rarely observed in *Zfp683*$^-$NK1.1$^+$ cells (Fig. 5 *A* and *B*). These data corroborate that ILC1s are a distinct lineage from NK cells. Of note, ∼30 to 50% of *Zfp683*$^+$ ILC1s were *Zfp683*$^{FM+}$, suggesting a partial efficiency in the recombination induced by *Zfp683*-driven Cre recombinase.

Since it was shown that human ILC1s can convert into ILC3s when cultured with IL-12, IL-23, and IL-1β (36), we next investigated whether this conversion occurs in vivo in our reporter mice. We examined the small intestine lamina propria, in which ILC3s are particularly abundant. First, we assessed the intracellular content of Rorγt and Eomes in Lin$^-$NKp46$^+$ cells of *Zfp683*^{FM} mice, which include ILC1s, NK cells, and NKp46$^+$NK1.1$^-$ ILC3s. *Zfp683*$^+$ (Tomato$^+$) ILC1s, Eomes$^+$ NK cells, and Rorγt$^+$ ILC3s appeared as distinct populations (Fig. 5*C*). However, ∼5 to 10% of Rorγt$^+$ ILC3s were *Zfp683*$^{FM+}$ (YFP$^+$) (Fig. 5 *D* and *E*), suggesting that a small percentage of ILC3s derive from ILC1s. None of the Eomes$^+$ cells were *Zfp683*$^{FM+}$, corroborating that ILC1s do not convert into NK cells. We conclude that in the small intestine only a limited percentage of ILC1s generate ILC3s, whereas ILC1s and NK cells remain distinct lineages.

NK Cells Express Hobit during MCMV Infection. Previous studies indicated that NK cells acquire phenotypical features of ILC1s in the tumor microenvironment (37, 38) and during *Toxoplasma gondii* infection (39). In these studies, the ILC1-like phenotype

was defined based on expression of CD49a, whereas Hobit expression was not assessed. We took advantage of our *Zfp683*^{Red} mice to study the expression pattern of Hobit during MCMV infection in spleen and liver NK1.1^{+}NKp46^{+} cells. Corroborating previous reports, CD49a was induced in spleen and liver NK cells as early as 1.5 d postinfection and continued to be expressed until 7 d postinfection (*SI Appendix*, Fig. S5). On day 1.5 postinfection, spleen and liver Eomes^{+} NK cells did not express *Zfp683*; however, *Zfp683* appeared in a significant fraction (15 to 30%) of Eomes^{+} NK cells on day 3.5 postinfection and persisted until day 7 postinfection (Fig. 6 *A*–*D*). Thus, NK cells can express *Zfp683* and CD49a during MCMV infection.

Consistent with previous studies (40), we observed that *Zfp683*$^{+}$ ILC1s in the liver went through a transient contraction phase at day 1.5 post–MCMV infection and returned to baseline levels in absolute numbers by day 3.5, whereas the numbers of Eomes^{+} NK cells expanded throughout (Fig. 6*E*). To test whether the initial ILC1 contraction was due to conversion of ILC1s into NK cells, we examined MCMV infection in *Zfp683*^{FM} mice. *Zfp683*$^{FM+}$ cells were exclusively present in the *Zfp683*$^{+}$ population at steady state and entirely disappeared on day 1.5 postinfection (Fig. 6 *F* and *G*), indicating that ILC1s remain distinct from NK cells also during MCMV infection.

To identify the cytokines that may control Hobit expression in NK cells, we isolated spleen NK cells from *Zfp683*^{Red} mice and cultured them with IL-2, IL-15, IL-12, transforming growth factor-beta (TGFβ), and IFNα, either alone or in different combinations. After 72 h, *Zfp683* was induced by IL-2 or IL-15 alone, and expression was further enhanced by TGFβ (Fig. 6 *H* and *I*). On the contrary, IFNα inhibited IL-2–mediated up-regulation of *Zfp683* expression. Although IL-12 is a proinflammatory cytokine that activates NK cells, it had no impact on *Zfp683* expression. Thus, while *Zfp683* is a faithful ILC1 marker in homeostasis, it is induced in NK cells in pathological conditions that generate an environment rich in cytokines such as IL-15, IL-2, and TGFβ.

It was previously shown that Hobit^{+} ILC1s provide a very early source of IFNγ for the control of MCMV in the liver 1 d after mice have been infected by hydrodynamic or intraperitoneal (i.p.) injection (8). Given that Hobit is also expressed in spleen and liver NK cells 3.5 d after infection, we wanted to evaluate whether Hobit deficiency impacts control of viral infection at a later time point when NK cells expand and become involved (41). *Zfp683*$^{fl/fl}$ *Ncr1*^{Cre} and control mice were infected i.p. with MCMV and viral titers were assessed in the liver and spleen at day 7. No major differences in viral titers were detected at this time point (*SI Appendix*, Fig. S5). We conclude that NK cell control of MCMV infection is Hobit-independent.

Discussion

Hobit is a transcriptional repressor encoded by *Zfp683* that has been proposed as a master transcription factor for tissue-resident memory T cells and ILC1s (18, 42). Using *Zfp683*^{Red} mice, we showed that the association of Hobit with ILC1s is tissue- and context-dependent. In liver and intestinal mucosa, *Zfp683* expression correlated well with ILC1s; however, *Zfp683* was coexpressed with Eomes in an ILC1-like NK cell subset uniquely present in salivary glands. Using *Zfp683*^{FM} mice, we corroborated that ILC1s and NK cells are distinct lineages in the steady state. However, *Zfp683* was induced in spleen and liver Eomes^{+} NK cells during MCMV infection and was up-regulated in vitro by cytokines, such as IL-15 and TGFβ that have been shown to induce markers of tissue residency (43). The impact of Hobit on ILC1s and NK cells was also tissue- and context-dependent. Comparing *Zfp683*$^{fl/fl}$ mice and *Zfp683*$^{fl/fl}$ *Ncr1*^{Cre} mice exposed the variable impacts of *Zfp683* deletion: a drastic reduction of Gzm ILC1s and IFNγ ILC1s in the liver; fewer ILC1s and more Eomes^{+} ILC1-like NK cells, along with decreased granzyme B production by ILC1s, in the salivary glands; and, solely, the reduction of granzyme B^{+} ILC1s in the small intestine lamina propria. *Zfp683* deletion did not affect the ability of NK cells to control MCMV infection in the liver at late time points, when NK cells are the major anti-MCMV effectors (41). We conclude that Hobit predominantly defines ILC1 programs and numbers, whereas it is less impactful when coexpressed with Eomes in ILC1-like NK cells and conventional NK cells.

A recently published study by Friedrich et al. showed that liver ILC1s encompassed a CD127^{+}TCF1^{hi} IFNγ^{+} subset and a CD127^{-}TCF1^{lo} cytotoxic subset and noted that germline *Zfp683* deletion increased the representation of the former versus the latter, indicating that CD127^{+}TCF1^{hi} IFNγ^{+} ILC1s are the progenitors of CD127^{-}TCF1^{lo} cytotoxic ILC1s and that Hobit is required for this transition (44). While our study identifies similar subsets of liver ILC1s, conditional deletion of *Zfp683* in the ILC1–NK lineage markedly reduced both subsets. Thus, our results are more consistent with the possibility that both IFNγ and Gzm ILC1 subsets develop from another progenitor through a Hobit-dependent process. The reason for the discrepancy between the two studies remains unclear. It should be noted that Friedrich et al. divided liver CD127$^{\pm}$TCF1^{hi} ILC1s into cKit^{+} and cKit^{-} subsets and indicated that the cKit^{-} subset was predominantly diminished by Hobit deficiency, while the cKit^{+} subset was unchanged. This latter subset may overlap with the *Rorc* ILC1 subset we detected in liver, which was unaffected by lack of Hobit and, in fact, relatively expanded under these conditions. Whether this *Rorc* ILC1 subset is a precursor developmentally related to other ILC1s, corresponds to a liver ILC1 progenitor recently identified (45), or encompasses exILC3s (29) remains to be investigated.

Hobit is a transcriptional repressor that inhibits the expression of molecules, such as the sphingosine-1-phosphate receptor, CCR7, and L-selectin, that mediate lymphocyte recirculation, facilitating the retention of a pool of memory T cells in tissues (46). Our study shows that Hobit is required for the presence of ILC1s in liver and, to a lesser extent, salivary glands. It remains unknown whether Hobit is necessary for the development of ILC1s or their retention in the tissue after they have developed. In the former case, Hobit may inhibit Eomes expression, directing a Tbet^{+} progenitor toward an ILC1 fate. In the latter case, one would expect ILC1s to be released from liver and salivary glands into the bloodstream in Hobit-deficient mice. In vivo imaging of tissue ILC1s will be essential to detect their movement in and out of tissues.

Beyond its function in tissue homing and retention, our study demonstrates that Hobit promotes expression of granzyme B while restraining expression of Eomes and TCF1. These effects are likely to be linked. It has been shown that TCF1 promotes Eomes expression in CD8 T cells (47). Moreover, TCF1 curbs the activity of a granzyme B–associated regulatory element, limiting granzyme B expression in TCF1-expressing NK cells (35). Thus, Hobit may directly inhibit expression of TCF1, causing reduced expression of Eomes and increased expression of granzyme B. This model is reminiscent of a similar role of Blimp, a Hobit homolog, in repressing TCF1 in NK cells (30). Thus, Hobit and Blimp may have parallel functions in controlling functional maturation of ILC1s and NK cells, respectively. Future epigenetic studies will be necessary to validate the presence of regulatory elements in the TCF1 region that are bound and repressed by Hobit. We do not exclude that Eomes and Hobit may also cross-regulate each other, as recently reported in CD8 T cells (48).

Although ILC1s have long been considered noncytotoxic, our study shows that ILC1s express granzymes A, B, and C.

Granzyme C seems to be uniquely expressed in ILC1s, whereas granzymes A and B are also present in cytotoxic NK cells. Since granzyme C is induced by TGFβ (37), its expression may reflect ILC1 location in TGFβ-rich tissue niches. ILC1s also expressed perforin mRNA, but to lower levels than NK cells, perhaps reflecting a lower cytotoxic capacity. However, Gzm ILC1s highly expressed the receptor for IL-21, a cytokine known to enhance NK cell cytotoxicity and inhibit NK cell survival and expansion (28). Thus, IL-21 may increase the lytic capacity of ILC1s while restraining their lifespan. ILC1s have previously been shown to provide an immediate source of IFNγ against MCMV infection in the liver upon hydrodynamic injection, which allows preferential delivery of virus to the liver (8). Although we found that Hobit expression was also induced in spleen and liver NK cells a few days after MCMV infection, Hobit deficiency had no effect on NK cell numbers or their ability to control MCMV infection in our model. It will be important to see whether Hobit impacts ILC1 or NK cell functions in other contexts, such as tumor growth and bacterial infections, or affects long-term memory of NK cells and ILC1s (49, 50).

ILCs have exhibited a certain degree of plasticity (1, 51, 52). Conversion of ILC3s into ILC1s has been shown both in vitro and in vivo using Rorγt fate-map mice (29, 53, 54). The reverse conversion from ILC1s to ILC3s has also been reported (36), although not formally demonstrated in an unperturbed system. Our analysis of *Zfp683*^{FM} mice demonstrates that some ILC3s, although *Zfp683*$^{-}$, have expressed *Zfp683* at a certain point, suggesting that they derive from ILC1s or from a *Zfp683*-expressing progenitor. In contrast, we saw no evidence for ILC1s converting into NK cells. These results corroborate the plasticity of ILCs and reaffirm ILC1s as a lineage distinct from NK cells.

Materials and Methods

Experimental details on animals, cell extraction from tissues, antibody staining for flow cytometry and sorting, cell culture and stimulations, scRNA-seq analyses, MCMV infection, and statistical analyses for this study are described in detail in *SI Appendix, Materials and Methods*.

All animal studies were approved by the Washington University Institutional Animal Care and Use Committee.

Data Availability. All scRNA-seq data reported in this paper have been deposited in the Gene Expression Omnibus (accession no. GSE185346).

All study data are included in the article and/or *SI Appendix*.

ACKNOWLEDGMENTS. We thank Richard M. Locksley for targeting vectors, and the Genome Technology Access Center at the McDonnel Genome Institute at Washington University for scRNA-seq on the 10X platform. The Genome Technology Access Center is supported in part by NCI Cancer Center Support Grant #P30 CA91842 to the Siteman Cancer Center at Washington University School of Medicine in St. Louis, MO and Grant# UL1TR002345 from the National Center for Research Resources (NCRR) to the Institute of Clinical and Translational Sciences (ICTS) at Washington University in St. Louis, MO. We thank E. Lantelme and D. Brinja and the Pathology and Immunology Flow Cytometry Core for cell sorting. This work was supported by Grants U01 AI095542, R01 DE025884, R01 AI134035, R01 DK124699, and U19 AI142733 (to M. Colonna) and NIH R01 AI130152 (to T.E.). K.Y. was supported by the Rheumatology Research Foundation Tobé and Stephen E. Malawista, MD Endowment in Academic Rheumatology and by Child Health Research Center K12.

1. M. Colonna, Innate lymphoid cells: Diversity, plasticity, and unique functions in immunity. *Immunity* **48**, 1104–1117 (2018).
2. E. Vivier *et al.*, Innate lymphoid cells: 10 years on. *Cell* **174**, 1054–1066 (2018).
3. G. F. Sonnenberg, M. R. Hepworth, Functional interactions between innate lymphoid cells and adaptive immunity. *Nat. Rev. Immunol.* **19**, 599–613 (2019).
4. L. Riggan, A. G. Freud, T. E. O'Sullivan, True detective: Unraveling group 1 innate lymphocyte heterogeneity. *Trends Immunol.* **40**, 909–921 (2019).
5. V. Stokic-Trtica, A. Diefenbach, C. S. N. Klose, NK cell development in times of innate lymphoid cell diversity. *Front. Immunol.* **11**, 813 (2020).
6. C. Seillet, L. Brossay, E. Vivier, Natural killers or ILC1s? That is the question. *Curr. Opin. Immunol.* **68**, 48–53 (2021).
7. G. Gasteiger, X. Fan, S. Dikiy, S. Y. Lee, A. Y. Rudensky, Tissue residency of innate lymphoid cells in lymphoid and nonlymphoid organs. *Science* **350**, 981–985 (2015).
8. O. E. Weizman *et al.*, ILC1 confer early host protection at initial sites of viral infection. *Cell* **171**, 795–808.e12 (2017).
9. S. Dadi *et al.*, Cancer immunosurveillance by tissue-resident innate lymphoid cells and innate-like T cells. *Cell* **164**, 365–377 (2016).
10. C. Di Censo *et al.*, Granzyme A and CD160 expression delineates ILC1 with graded functions in the mouse liver. *Eur. J. Immunol.* **51**, 2568–2575 (2021).
11. L. Krabbendam, J. H. Bernink, H. Spits, Innate lymphoid cells: From helper to killer. *Curr. Opin. Immunol.* **68**, 28–33 (2021).
12. M. M. Rahim, A. P. Makrigiannis, Ly49 receptors: Evolution, genetic diversity, and impact on immunity. *Immunol. Rev.* **267**, 137–147 (2015).
13. C. L. Kirkham, J. R. Carlyle, Complexity and diversity of the NKR-P1:Clr (Klrb1:Clec2) recognition systems. *Front. Immunol.* **5**, 214 (2014).
14. M. G. Constantinides, B. D. McDonald, P. A. Verhoef, A. Bendelac, A committed precursor to innate lymphoid cells. *Nature* **508**, 397–401 (2014).
15. C. S. N. Klose *et al.*, Differentiation of type 1 ILCs from a common progenitor to all helper-like innate lymphoid cell lineages. *Cell* **157**, 340–356 (2014).
16. W. Xu *et al.*, An Id2^{RFP}-reporter mouse redefines innate lymphoid cell precursor potentials. *Immunity* **50**, 1054–1068.e3 (2019).
17. J. Zhang *et al.*, T-bet and Eomes govern differentiation and function of mouse and human NK cells and ILC1. *Eur. J. Immunol.* **48**, 738–750 (2018).
18. L. K. Mackay *et al.*, Hobit and Blimp1 instruct a universal transcriptional program of tissue residency in lymphocytes. *Science* **352**, 459–463 (2016).
19. A. P. McFarland *et al.*, Multi-tissue single-cell analysis deconstructs the complex programs of mouse natural killer and type 1 innate lymphoid cells in tissues and circulation. *Immunity* **54**, 1320–1337.e4 (2021).
20. V. S. Cortez, A. Fuchs, M. Cella, S. Gilfillan, M. Colonna, Cutting edge: Salivary gland NK cells develop independently of Nfil3 in steady-state. *J. Immunol.* **192**, 4487–4491 (2014).
21. D. K. Sojka *et al.*, Tissue-resident natural killer (NK) cells are cell lineages distinct from thymic and conventional splenic NK cells. *eLife* **3**, e01659 (2014).
22. M. L. Redhead *et al.*, The transcription factor NFIL3 is essential for normal placental and embryonic development but not for uterine natural killer (UNK) cell differentiation in mice. *Biol. Reprod.* **94**, 101 (2016).
23. D. M. Gascoyne *et al.*, The basic leucine zipper transcription factor E4BP4 is essential for natural killer cell development. *Nat. Immunol.* **10**, 1118–1124 (2009).
24. S. Kamizono *et al.*, Nfil3/E4bp4 is required for the development and maturation of NK cells in vivo. *J. Exp. Med.* **206**, 2977–2986 (2009).
25. C. Seillet *et al.*, Nfil3 is required for the development of all innate lymphoid cell subsets. *J. Exp. Med.* **211**, 1733–1740 (2014).
26. T. L. Geiger *et al.*, Nfil3 is crucial for development of innate lymphoid cells and host protection against intestinal pathogens. *J. Exp. Med.* **211**, 1723–1731 (2014).
27. X. Yu *et al.*, The basic leucine zipper transcription factor NFIL3 directs the development of a common innate lymphoid cell precursor. *eLife* **3**, e04406 (2014).
28. M. T. Kasaian *et al.*, IL-21 limits NK cell responses and promotes antigen-specific T cell activation: A mediator of the transition from innate to adaptive immunity. *Immunity* **16**, 559–569 (2002).
29. C. S. Klose *et al.*, A T-bet gradient controls the fate and function of CCR6-RORγt^{+} innate lymphoid cells. *Nature* **494**, 261–265 (2013).
30. P. L. Collins *et al.*, Gene regulatory programs conferring phenotypic identities to human NK cells. *Cell* **176**, 348–360.e12 (2019).
31. C. N. Skon *et al.*, Transcriptional downregulation of S1pr1 is required for the establishment of resident memory CD8^{+} T cells. *Nat. Immunol.* **14**, 1285–1293 (2013).
32. M. J. van Helden *et al.*, Terminal NK cell maturation is controlled by concerted actions of T-bet and Zeb2 and is essential for melanoma rejection. *J. Exp. Med.* **212**, 2015–2025 (2015).
33. N. M. Adams *et al.*, Transcription factor IRF8 orchestrates the adaptive natural killer cell response. *Immunity* **48**, 1172–1182.e6 (2018).
34. E. M. Mace *et al.*, Biallelic mutations in IRF8 impair human NK cell maturation and function. *J. Clin. Invest.* **127**, 306–320 (2017).
35. B. Jeevan-Raj *et al.*, The transcription factor Tcf1 contributes to normal NK cell development and function by limiting the expression of granzymes. *Cell Rep.* **20**, 613–626 (2017).
36. J. H. Bernink *et al.*, Interleukin-12 and -23 control plasticity of CD127(+) group 1 and group 3 innate lymphoid cells in the intestinal lamina propria. *Immunity* **43**, 146–160 (2015).
37. V. S. Cortez *et al.*, SMAD4 impedes the conversion of NK cells into ILC1-like cells by curtailing non-canonical TGF-β signaling. *Nat. Immunol.* **18**, 995–1003 (2017).
38. Y. Gao *et al.*, Tumor immunoevasion by the conversion of effector NK cells into type 1 innate lymphoid cells. *Nat. Immunol.* **18**, 1004–1015 (2017).
39. E. Park *et al.*, *Toxoplasma gondii* infection drives conversion of NK cells into ILC1-like cells. *eLife* **8**, e47605 (2019).
40. G. Dodard *et al.*, Inflammation-induced lactate leads to rapid loss of hepatic tissue-resident NK cells. *Cell Rep.* **32**, 107855 (2020).

41. V. C. Lam, L. L. Lanier, NK cells in host responses to viral infections. *Curr. Opin. Immunol.* **44**, 43–51 (2017).
42. S. Zundler *et al.*, Hobit- and Blimp-1-driven $CD4^+$ tissue-resident memory T cells control chronic intestinal inflammation. *Nat. Immunol.* **20**, 288–300 (2019).
43. L. K. Mackay *et al.*, T-box transcription factors combine with the cytokines TGF-β and IL-15 to control tissue-resident memory T cell fate. *Immunity* **43**, 1101–1111 (2015).
44. C. Friedrich *et al.*, Effector differentiation downstream of lineage commitment in ILC1s is driven by Hobit across tissues. *Nat. Immunol.* **22**, 1256–1267 (2021).
45. L. Bai *et al.*, Liver type 1 innate lymphoid cells develop locally via an interferon-γ-dependent loop. *Science* **371**, eaba4177 (2021).
46. D. Masopust, A. G. Soerens, Tissue-resident T cells and other resident leukocytes. *Annu. Rev. Immunol.* **37**, 521–546 (2019).
47. Z. Chen *et al.*, TCF-1-centered transcriptional network drives an effector versus exhausted CD8 T cell-fate decision. *Immunity* **51**, 840–855.e5 (2019).
48. L. Parga-Vidal *et al.*, Hobit identifies tissue-resident memory T cell precursors that are regulated by Eomes. *Sci. Immunol.* **6**, eabg3533 (2021).
49. A. M. Mujal, R. B. Delconte, J. C. Sun, Natural killer cells: From innate to adaptive features. *Annu. Rev. Immunol.* **39**, 417–447 (2021).
50. O. E. Weizman *et al.*, Mouse cytomegalovirus-experienced ILC1s acquire a memory response dependent on the viral glycoprotein m12. *Nat. Immunol.* **20**, 1004–1011 (2019).
51. S. M. Bal, K. Golebski, H. Spits, Plasticity of innate lymphoid cell subsets. *Nat. Rev. Immunol.* **20**, 552–565 (2020).
52. P. Bielecki *et al.*, Skin-resident innate lymphoid cells converge on a pathogenic effector state. *Nature* **592**, 128–132 (2021).
53. M. Cella, K. Otero, M. Colonna, Expansion of human NK-22 cells with IL-7, IL-2, and IL-1beta reveals intrinsic functional plasticity. *Proc. Natl. Acad. Sci. U.S.A.* **107**, 10961–10966 (2010).
54. M. Cella *et al.*, Subsets of ILC3-ILC1-like cells generate a diversity spectrum of innate lymphoid cells in human mucosal tissues. *Nat. Immunol.* **20**, 980–991 (2019).